Simplified equivalent finite element modelling of concrete-filled steel tubular K-joints with and without studs

Marco Filippo Ferrotto [a], Luigi Fenu [b], Jun-Qing Xue [c, d*], Bruno Briseghella [c, d], Bao-Chun Chen [c, d], Liborio Cavaleri [a]

[a] Department of Engineering, University of Palermo, Palermo, 90128, Italy

[b] Department of Civil Engineering, Environment and Architecture, University of Cagliari, Cagliari, 09123, Italy

[c] College of Civil Engineering, Fuzhou University, Fuzhou, 350108, China.

[d] Fujian Provincial Key Laboratory on Multi-disasters Prevention and Mitigation in Civil Engineering, Fuzhou University, Fuzhou, 350108, China.

*Corresponding author, e-mail: junqing.xue@fzu.edu.cn

Abstract

Concrete Filled Steel Tubular (CFST) K-joints employed for truss structures gained high interest in the last years due to their widespread use in engineering practice. The overall performances of these joints can be efficiently improved by using steel studs welded in the inner surface of the steel chord filled with the concrete, avoiding punching shear failure, and improving the overall strength and ductility. However, a reliable prediction of the structural behavior of the joints is outmost of importance for the assessment of the capacity of new and existing structures, and there are no standardized design methods nowadays. In this paper, the structural performances of CFST K-joints with and without steel studs are investigated by Finite Element Modelling (FEM) approach with the aim to provide a predictive tool for the design. A comprehensive discussion of the key parameters that govern the FEM procedure as well as the calibration of the FE models was provided to give the basis for a reliable modelling of CFST K-joints with and without studs for the predictions of the load-displacement/strain response and the strength, considering the main failure mechanisms. In this context, in addition to the detailed FEM of CFST K-joints with steel studs, a simplified

equivalent FEM approach is proposed to reduce computational effort keeping the same accuracy.

Keywords: concrete filled steel tubes (CFST); K-joints; finite element modelling (FEM); simplified equivalent modelling; steel studs.

1. Introduction

Truss structures made by concrete filled steel tubular (CFST) members have been studied and widely used in engineering practice in the last twenty years. Many examples of constructions show the high mechanical performances of the tubular shape regarding loading in compression, torsion and bending [1-5] as well as for the benefit from the light self-weight. The CFST structures have high strength and ductility due to the compressive strength and ductility of the core concrete increased by the confinement provided by the steel tube. A number of studies were dedicated to the assessment and the design of the capacity of steel hollow members and joints with and without concrete filling [6-16].

The design of members in truss structures is generally based on yielding conditions since the deformation over the yielding point could become excessive. Another aspect is that the failure conditions need to be accurately studied, because, for example, a tensile member made of ductile steel can be brittle if a particular cross section is weakened, e.g., by holes in such a way that this cross section fails before the whole member yields. It is therefore required that yielding occurs first. The challenge in the optimization of the design procedure leads to a correct definition of the joint connections. However, the research in this direction is not exhaustive and needs further development from an analytical and experimental point of view. For the latter, the difficulties are addressed to the realization of full-scale specimens and related experimental setup. On this aim, Finite Element Modelling (FEM) approach can be a powerful tool for the prediction of the capacity of a wide range of configurations of such kind of composite joints, given that the FE models are accurately calibrated before.

Among the most important studies available in the state of the art, some experimental and numerical researches on the mechanical performance and failure modes of local joints in truss structures were conducted. Sakai et al. [17] carried out an experimental study on tubular K-joints of truss girder to investigate on the ultimate strength and fatigue properties on six different types of specimens, composed of concrete non-filled, concrete filled, and concrete filled with reinforcement. It can be found that the strength and the stiffness of the concrete filled specimens was considerably improved with respect to K-joints made only with Circular Hollow Sections (CHS). Huang et al. [9] carried out experimental research on the failure modes of K-joints of CFST truss structures of a tubular chord filled with concrete and two braces inclined at the same angle with respect to the chord. The results were compared with those obtained by testing K-joint specimens of CHS truss structures with the same size. It can be confirmed that in the case of CHS K-joints a chord face failure mode occurred, while for CFST K-joints the mechanical performances were noticeably improved despite the failure by punching shear in the tension region was observed. It can be demonstrated also that the performances of the K-joints can be considerably improved in the case of using internal steel studs welded in the inner surface of the chord in the joint region. Liu et al. [18] performed an experimental investigation on K-joints of CFST members with and without inner studs, following the same experimental setup by Huang et al. [9]. Specimens with different dimensions were used for the testing, confirming the results of the previous experimental study in terms of failure mechanisms. Hou et al. [19,20] carried out experimental and numerical investigations on Concrete Filled Double Steel Tube (CFDST) K-joints. The members were realized by using inner and outer steel tubes with sandwiched filled concrete in between and subjected to different load paths. Finally, simplified analytical formulations were proposed for the prediction of the strength. Jin et al. [21] presented a numerical study on blind-bolted demountable CFST K-joints on square hollow sections. The K-joint specimens were realized by concrete filled chord, hollow braces, flush endplate, blind bolts, and through-wall bolts. The authors discussed on the mechanical

performances of such composite joints and gave some geometrical and mechanical design recommendations for the components of the joints based on the numerical observations. Zeng et al. [22] presented the numerical studies to determine the stress concentration factors in the joint region for several configurations of CFST K-joints subjected to different boundary conditions. It can be highlighted that hot spot stresses for CFST K-joints resulted to be lower than those of hollow specimens and identified four geometrical parameters that govern the failure modes of such joints. Hou et al. [23,24] investigated and compared the local bearing forces of CFST members with vertical or inclined brace by experimental and FEM approaches. It can be highlighted the role of the concrete filling and the typical failure modes of T-joints with different inclinations of the steel brace with respect to the steel chord. Zeng et al. [25] presented the numerical studies to determine the stress concentration factors in the joint region for several configurations of CFST T-joints subjected to different boundary conditions.

Besides the researches on the local joints, the mechanical performance and failure modes of truss structures were also investigated. Huang et al. [11] carried out experimental research on the joint resistance and failure modes of CHS, hybrid with an upper CFST chord and a lower CHS chord, and CFST trusses with different web arrangements. It can be found that CFST girder joints fail via punching shear, except when brace failure occurs first. The formulae, originally proposed for CHS joints in some codes, was updated to calculate the resistance of CFST joints. Huang et al. [26] carried out experimental research on 1:8 scale two-span specimen designed for multi-shaking table test under artificial waves based on design spectrum to investigate the seismic behaviour, based on a continuous bridge with CFST composite truss girders and lattice high pier as prototype. The FE model was developed by using OpenSees software, and the accuracy was verified by shacking table test results. Xu et al. [27] investigated the effect of the rise-to-span ratio and infill concrete on the flexural performance of curved concrete filled steel tubular (CCFST) trusses with curved CFST chords and hollow braces by experimental and FEM approaches. Different failure

100 modes were observed: bending failure for CFST trusses, bending-shear failure for CCFST trusses
101 and local buckling failure for hollow tubular trusses. It can be found that the stiffness and
102 load-carrying capacity of CCFST trusses were larger than those of CFST trusses, but the CCFST
103 trusses experienced a joint failure with relatively low ductility, resulting in a sudden drop of
104 strength. Meanwhile, the infill concrete provided support to the steel tubular chords and increased
105 the stiffness, load-carrying capacity and ductility. The simplified models for predicting the elastic
106 stiffness and the load-carrying capacity were suggested. Yuan et al. [28] presented an experimental,
107 numerical (OpenSees) and theoretical study on the seismic performance of CFST battened built-up
108 column (CFST-BBC) piers. The failure modes of CFST-BBC specimens were dominated by local
109 buckling at the bottom of CFST chords. The theoretical methods to calculate the elastic lateral
110 stiffness, the peak lateral load, the peak and ultimate drift ratios on the top of the CFST-BBC piers
111 were proposed and verified by the test data and FEM analysis results.

112 Usually, experimental tests give a fundamental benchmark to confirm the reliability of the
113 proposed predictive analytical models. However, there is a lack in the number of available
114 experimental data, and the available experimental studies do not cover the geometrical and
115 mechanical ranges of use of such kind of composite joints. Moreover, for specific joint
116 configuration, i.e. in the presence of steel studs, the definition of accurate predictive models is
117 difficult by using analytical approach. FEM is a powerful approach for the prediction of the
118 capacity of joint members and provides a strong help to fill the gap of experimental database. On
119 the other hand, FE models need to be carefully calibrated based on experimental results to be used
120 as predictive approach in order to give a reliable prediction of the capacity. The OpenSees software
121 was used by some researchers to build the fibre-based FE model of CFST truss structure. However,
122 the influence of the interaction between the steel tube and core concrete was neglected. In order to
123 analyse in detail the interaction between the steel tube and core concrete also considering the steel
124 studs, the ABAQUS software was used, building up the FE model of CFST truss structure with

125 solid elements. In this context, in addition to the mechanical behaviour of the elements (concrete
126 core, steel chord and braces) that compose the joint, also the interaction between the contact
127 surfaces (steel and concrete) is considered in the FE model.

128 The aim of this study is therefore to provide a reliable FEM tool for i) the prediction of the
129 load-displacement/strain (stiffness) response and ii) the strength prediction of the K-joints with and
130 without steel studs, considering, according to the Eurocode 3 [29], the main failure conditions of the
131 joints identified by:

132 - Chord face failure (chord face plasticization);

133 - Punching shear failure of the chord wall (crack initiation leading to rupture of the brace
134 members from the chord member);

135 - Local buckling failure of a brace member or of a chord member at the joint location;

136 - Brace failure with reduced effective width (cracking in the welds or in the brace members).

137 Experimental tests by Huang et al. [9] and Liu et al. [18] were used in this study both for the
138 calibration of the numerical model and subsequently for the prediction of the capacity. Main
139 characteristics of the experimental specimens, such as geometrical, mechanical properties and load
140 paths, are described in the following before introducing the description of the path of the FEM
141 carried out by the Simulia ABAQUS Software package [30].

142 In a first phase, the attention is dedicated to the calibration of the failure conditions of the CHS
143 and CFST K-joints. Subsequently, the FE model of CFST K-joints with steel studs welded to the
144 interior surface of the chord in the joint region (CFST-S) is built up based on the actual
145 reproduction of experimental specimens. Then, a simplified equivalent modelling approach is
146 proposed to reduce the complexity of the FE models and the computational efforts. The above
147 findings are then used for the comparisons with other experimental results to demonstrate the
148 reliability of the proposed FE model in the prediction of the strength and the stiffness properties of
149 the composite K-joints.

2. CFST K-joints: description of the specimens

According to the test setup by Huang et al. [9] and Liu et al. [18], the two steel brace members were connected by welding with a chord member. The inclination of the brace with respect to the center line of the chord member was 60°, and their centerlines met each other along the vertical centerline of the chord member to eliminate eccentricity. The lengths of the chord and brace members were l_0 = 2000 and l = 900 mm, respectively. The outer diameter and thickness for the chord were d_0 = 510 mm and t_0 = 10 mm, respectively. The brace members (thickness t = 6 mm, 8 mm, and 10 mm) had an outer diameter of d = 219 mm. The minimum distance (gap) between the outer surfaces along the surface of the chord member was g = 42 mm. The member sizes and the mechanical characteristics of the steel and the concrete of all tubular K-joint specimens under consideration are listed in Table 1.

Regarding the load paths, the steel chord was subjected to compression force in the first step. Then, the load was kept constant during the second step in which the steel braces were subjected one in tension and the other one in compression simultaneously (Fig. 1). The compression force at the top of the chord was 2500 kN and of 4800 kN for the CHS and the CFST specimens, respectively. The boundary conditions can be schematized in Fig. 1. Please refer to the original treatment for more details [9,18].

Steel studs with a height of 80 mm were used (shank diameter = 19 mm, head diameter = 32 mm, head thickness = 12 mm) to build up CFST-S specimens. The stud spacing in the direction of the chord tube was 150 mm, and the spacing along the interior circumference of each chord section was 128 mm (12 studs per section). The spacing in the longitudinal direction was 150 mm and the studs were welded on eight circular sections of the chord tube. Therefore, in each joint, 96 studs were welded along 1050 mm (details in Fig. 2).

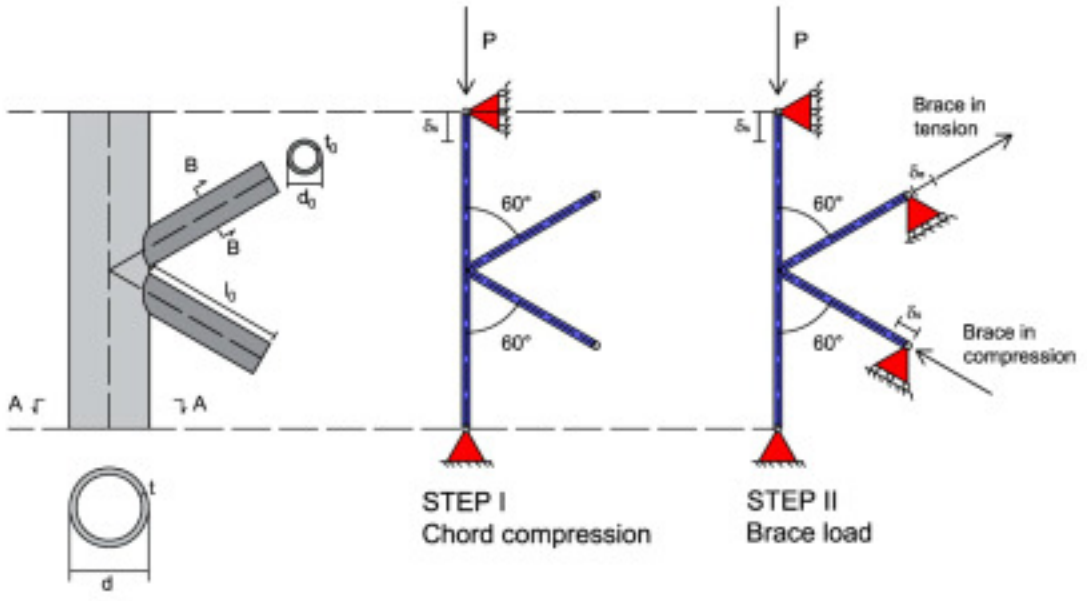

173

174 Fig. 1. Experimental setup and boundary condition for CHS, CFST and CFST-S K-joints [9,18]

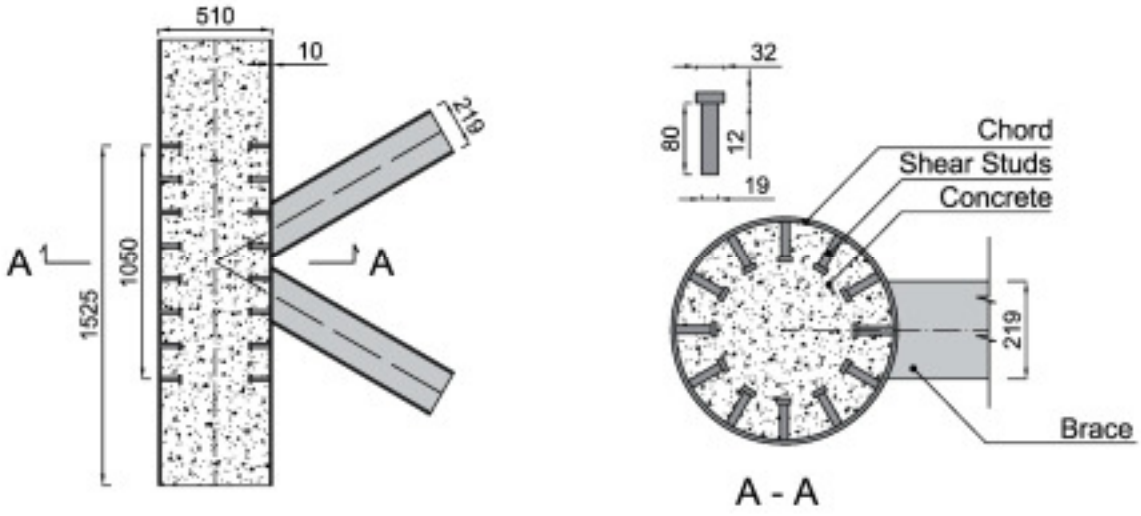

175

176 Fig. 2. Details of CFST-S specimens [9]

177 The experimental tests showed different failure mechanisms for the specimens. CHS K-joints
178 failed by chord face failure mode, while CFST and CFST-S K-joints failed by punching shear in the
179 joint region of the weld toe with the brace in tension except for the case of specimens with low
180 thickness to diameter ratio for the braces (as for CFST-6 specimen), for which buckling in
181 compression was observed and identified as failure mode. In the other specimens, brace failure was
182 caused by yielding at the joint location, with an outward bulge that formed close to the joint (Fig. 3).

Finally, it could be stated that punching shear failure was found to be the typical failure mode of CFST K-joints if no brace failure mode occurred before. The main difference, in the case of studs, is that the specimens reach the yielding strength of the steel for the brace in tension. Results are shown in Table 2 and Fig. 4.

Table 1

Geometrical and mechanical characteristics of the CFST K-joints [9,18]

Source	Specimen Label	Geometry/mm		Steel/MPa		Concrete/MPa
		Chord $d \times t \times l$	Braces $d_0 \times t_0 \times l_0$	Chord f_y - f_u	Braces f_y - f_u	f_c
Huang et al. [9]	CHS-6	510×10×2000	219×6×820	311 - 425 ε_f = 0.33	330 - 485 ε_f = 0.21	/
	CFST-6					37
	CFST-6 S*					
	CHS-8	510×10×2000	219×8×820		325 - 490 ε_f = 0.22	/
	CFST-8					37
	CFST-8 S*					
	CFST-10	510×10×2000	219×10×820		322 - 487 ε_f = 0.21	37
	CFST-10 S*					
Liu et al. [18]	PI*	600×14×2000	245×10×900	275 - 428 ε_f = 0.33	259 - 417 ε_f = 0.22	39
	PII					

* Specimens with studs. f_y is the yielding strength of steel; f_u is the ultimate tensile strength of steel; ε_f is the failure strain of the steel; f_c is the cylinder compressive strength of concrete.

Table 2

Comparison between experimental failure and yielding force for the braces in tension

Specimen Label	Exp - brace in tension/kN	Yield strength/kN	Exp/Yield strength	Failure mechanism
CHS-6	717	1324	0.54	CF
CFST-6	1118	1325	0.84	B / PS
CFST-6 S*	1334	1325	1.01	B / PS
CHS-8	719	1723	0.42	CF
CFST-8	1535	1723	0.89	PS
CFST-8 S*	1761	1723	1.02	PS
CFST-10	1611	2114	0.76	PS
CFST-10 S*	2120	2114	1.00	PS
PI*	2080	1912	1.09	PS
PII	1847	1912	0.97	PS

CF=Chord failure; B=Buckling of the compressed brace; PS=Punching shear.

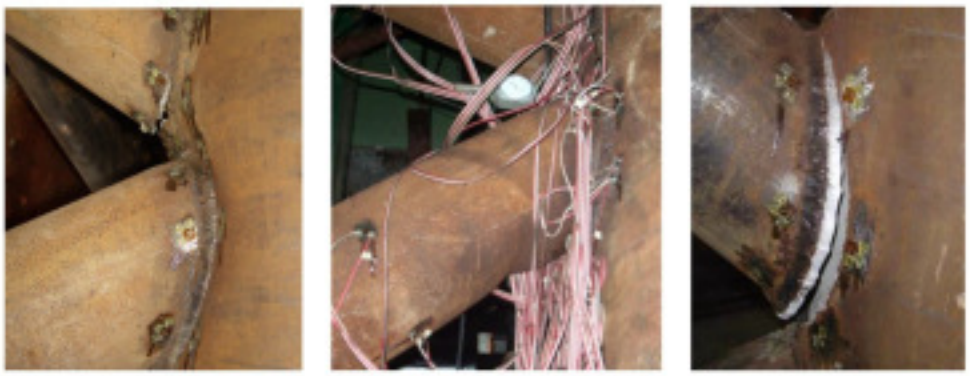

(a) (b) (c)

Fig. 3. Failure modes: (a) chord failure; (b) buckling of the compressed brace; (c) punching shear [9]

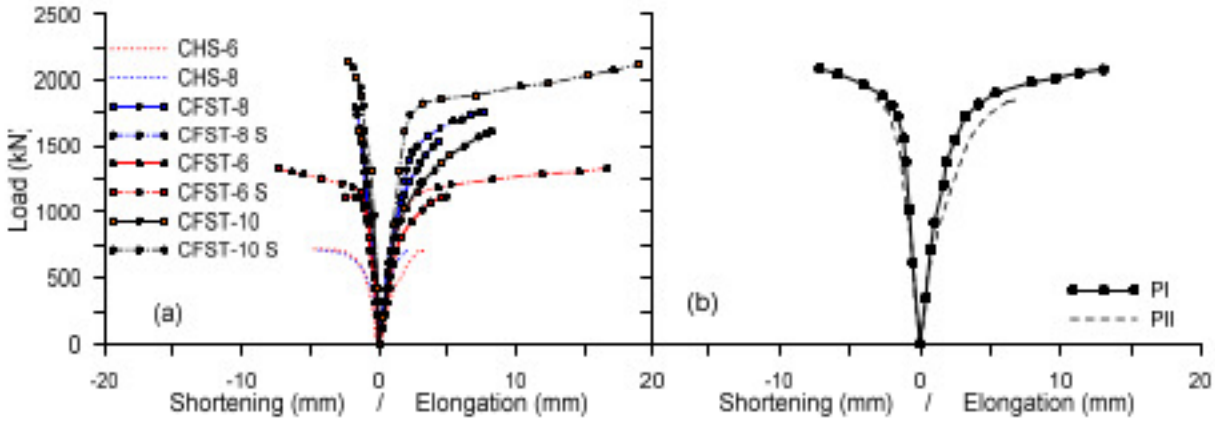

Fig. 4. Experimental data by (a) Huang et al. [9] and (b) Liu et al. [18]

3. Finite Element Modelling

As stated in the previous sections, the aim of the study is to address a reliable FEM approach to predict the capacity in terms of strength and stiffness for CFST K-joints with and without steel studs. In the frame of modelling CFST K-joints with studs, a simplified FEM procedure is proposed to reduce the high time-computational effort keeping the same accuracy in the results.

The FEM software package Simulia ABAQUS CAE [30] was used to build up the FE models for K-joints. The analysis was performed in two steps according to the test setup discussed in Section 2. Firstly, the steel chord was loaded up to a pre-fixed compressive load. Then, the load was

kept constant, and the steel braces were loaded until the failure of the joint. Static non-linear analysis was defined by considering geometrical and mechanical non-linearity of the members.

Four types of FE models for the K-joints were built, that are:

1. K-joint FE model with CHS.
2. K-joint FE model with CFST.
3. Detailed actual K-joint FE model with studs (CFST-S).
4. Simplified equivalent K-joint FE model with studs.

3.1 Element modelling and boundary conditions

For the FE model built for CFST K-joints without steel studs, the concrete filling inside the steel chord was modelled by means of C3D8-R (8-node linear brick, reduced integration, hourglass control) elements, while the steel chord and braces were modelled by means of C3D10 (10-node quadratic tetrahedron) elements. In the case of the FE model built for the specimens with studs, C3D10 elements were used to model the concrete, steel chord and braces, and studs. In the latter case, a slice of the complete model was built to reduce computational efforts, as shown in Figs. 5-7. The reason of using C3D10 elements is due to the complex shape of the studs and the concrete for CFST-S specimens. It is worth to state that in the frame of a simplified FEM, in this work, the weld toe was not included in the FE model.

Surface-to-surface contact interactions were defined between the inner surface of the steel chord and the concrete filling. "Hard contact" was set in the normal direction, allowing separation after contact during the sliding, while "penalty contact" was defined in the tangential directions, assuming friction coefficient of 0.5 according to references [20,31].

Boundary conditions were assumed in accordance with the experimental setup and load paths of Fig. 1. In detail, the specimens were clamped at one side of the chord end. The other side was loaded in the axis direction in the first stage of preloading of the steel chord. At the point load, the displacements in the orthogonal directions were fixed. In the first step the steel braces were not

constrained. In the brace load step, the steel braces were fixed in the direction orthogonal to the axis and a displacement was applied at the centre of the end cross section to a reference point pinned by a rigid body.

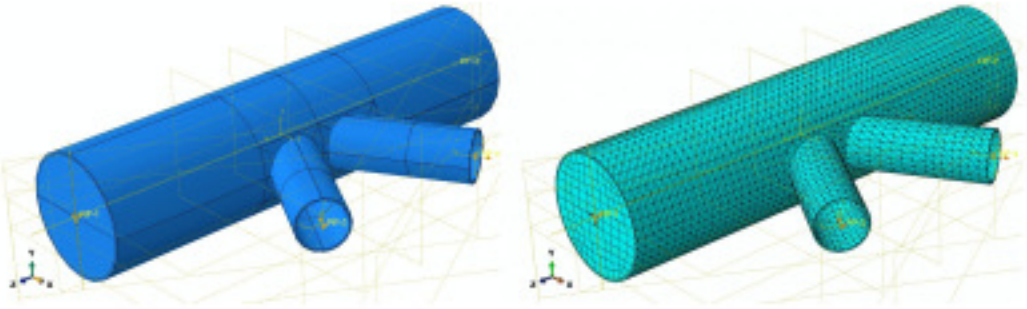

Fig. 5. Assembly model and meshing for CFST K-joint specimens.

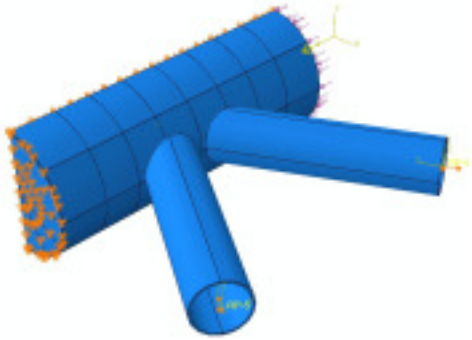

Fig. 6. Boundary conditions for the actual slice model of CFST K-joint specimens with steel studs

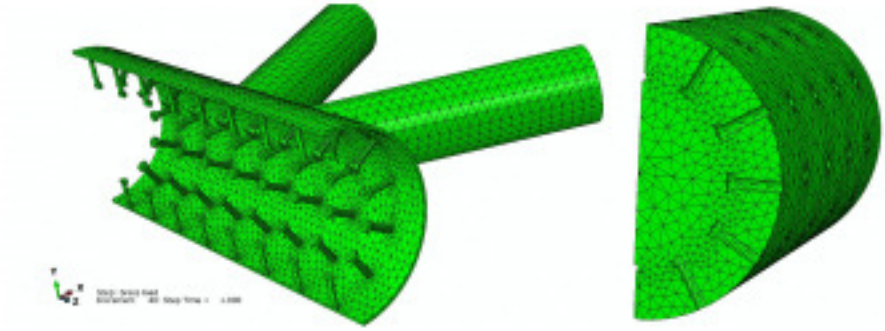

Fig. 7. Steel and concrete meshing for CFST K-joint specimens with studs

3.2 Material modelling

Modelling of Steel

The constitutive behaviour of the steel was assumed by elasto-plastic stress-strain relation

model with hardening, according to the experimental data in Huang et al. [9] and Liu et al. [18] (see Table 1). The modulus of elasticity and the Poisson's ratio for the steel were 206000 MPa and 0.3, respectively.

Modelling of concrete

The concrete damage plasticity (CDP) model provided in ABAQUS was used to define the material behaviour of the concrete in CFST chords. By using the plasticity model available in ABAQUS, it was possible to consider concrete cracking in tension as well as crushing in compression. Formulations defining the behaviour of concrete under multi-axial stress state include the yield criterion, the flow rule and the hardening/softening rule that defines the non-linear behaviour of concrete. The above formulations depend by the plasticity parameters, that are the dilation angle (ψ) that defines the plastic flow potential, the ratio between the compressive strength under biaxial loading and uni-axial compressive strength (f_{b0}/f_{c0}), the flow potential eccentricity (e), the viscosity parameter (μ) and the ratio (K_c) between the second stress invariant on the tensile meridian and that on the compressive meridian for the yield function. The uniaxial stress-strain relation proposed by Han et al. [32] (Eq. 1) was adopted to simulate the behaviour of the concrete under compression according to several other studies [19,21].

$$\sigma_c(\varepsilon) = f_{c0}\begin{cases} 2\dfrac{\varepsilon}{\varepsilon_0} - \left(\dfrac{\varepsilon}{\varepsilon_0}\right)^2 & \varepsilon \le \varepsilon_0 \\ \dfrac{\varepsilon}{\varepsilon_0}\dfrac{1}{\beta\left(\dfrac{\varepsilon}{\varepsilon_0}-1\right)^2 + \dfrac{\varepsilon}{\varepsilon_0}} & \varepsilon > \varepsilon_0 \end{cases} \quad (1)$$

where, $\sigma_c(\varepsilon)$ is the current compressive stress ε is the current strain, ε_0 is the strain at peak strength and β is a parameter that depends on the confinement mechanical ratio ξ, to be determined as follows (Eqs. 2~5):

$$\varepsilon_0 = \varepsilon_c + 800\xi^{0.2} \times 10^{-6} \quad (2)$$

$$\varepsilon_c = (1300 + 12.5 f_{c0}) \times 10^{-6} \quad (3)$$

$$\beta = \left(2.36 \times 10^{-5}\right)^{\left[0.25 + (\xi - 0.5)^2\right]} f_{c0}^{\ 0.5} \geq 0.12 \quad (4)$$

$$\xi = \frac{A_s}{A_c} \frac{f_y}{f_{c0}} \quad (5)$$

Please refer to the original treatment of Han et al. [32] for additional details of the formulae employed. Fig. 8 (a) and (b) shows the uniaxial constitutive stress-strain laws for the concrete related to the two experimental data considered in this study [9, 18]. It has to be stated that, although it is well known that generally confinement effects for concrete filled steel tube columns subjected mainly to axial compression loads (for compression stresses higher than 50% of f_{c0}), confinement effects as well as stress-path dependency play significant role in the strength and ductility enhancement of such columns [33-38]; for the specimens considered in the frame of this study, the concrete inside the steel chord of the K-joint, there is no high level of compression stress so the confinement effects are not predominant in the global response of the K-joints. This can be simple highlighted by evaluating the compressive stress in the concrete of the chord in the first stage of loading of the experimental test, which is the loading of the steel chord. For the specimens by Huang et al. [9], the preload of 4800 kN on specimens CFST-6, CFST-8 and CFST-10 (this applies also for specimens with studs named "S") causes a compressive stress level in the concrete of around 16 MPa in view of a uniaxial cylindrical compressive strength of 37 MPa; while for the specimens by Liu et al. [18], the compressive stress level in the concrete results around 12 MPa, in view of a uniaxial cylindrical compressive strength of 39 MPa, resulting therefore in both cases lower that the 50% of f_{c0}.

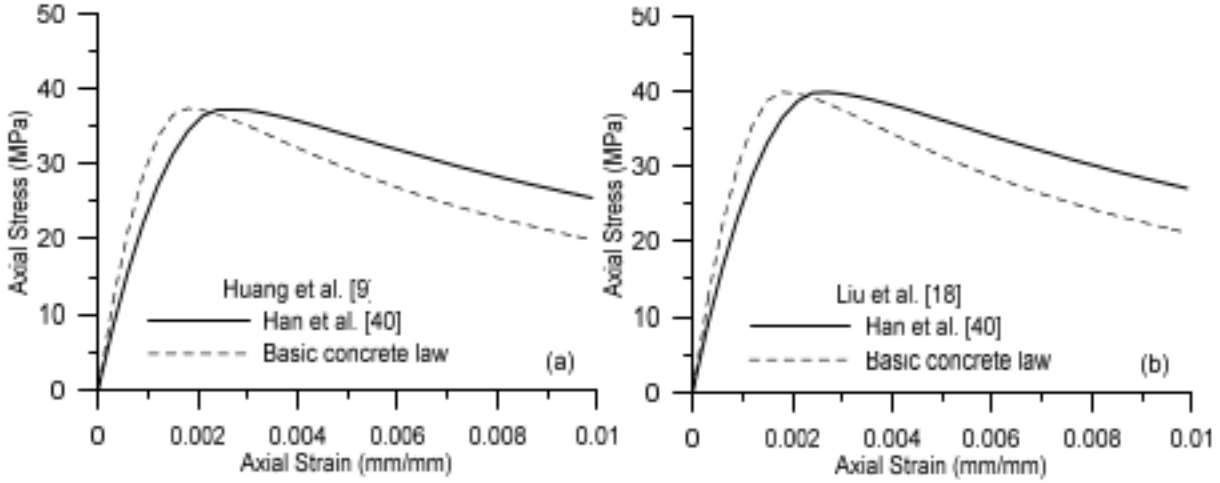

Fig. 8. Uni-axial compressive stress-strain law for the concrete: (a) Huang et al. [9] and (b) Liu et al. [18]

Based on the above considerations, and since it was noticed by the numerical simulations that the concrete did not reach high stresses levels, the definition of the plasticity parameters was set by the usually default values (see Table 3).

Table 3

Plasticity parameters used for the concrete in CDP model

ψ	f_{b0}/f_{c0}	e	K_c	μ
33°	1.16	0.1	0.667	0.0001

Regarding the behavior in tension of the concrete, according to Tao et al. [39] a linear uniaxial tensile stress up to the reaching of the tensile strength (assumed 10% of f_{c0}) is defined followed by the softening response, defined by means of fracture energy G_F (Eq. 6), depending on f_{c0} and the maximum coarse aggregate size d_0 (assumed 20 mm if no specified)

$$G_F = \left(0.0469 \cdot d_0^2 - 0.5 \cdot d_0 + 26\right)\left(0.1 f_{c0}\right)^{0.7} \quad [N/m] \tag{6}$$

296 ## 4. Finite element modelling results

297 ### 4.1 CHS and CFST specimen failure calibration

298 The stiffness distribution in combination with the material behavior determined the failure
299 mode for the K-joints. The lowest failure load for all these failure modes gave the governing
300 strength. It was observed also by experimental results, that the failure for CHS specimens by Huang
301 et al. [9] was identified by chord failure, while for CFST, the failure was identified by punching
302 shear.

303 These failure mechanisms are associated with a plastic strain failure lower than the rupture
304 strain of the steel material itself. To reproduce the physical failure, detailed modelling of the
305 welding toe and failure conditions should be accurately defined. This requires high computational
306 effort by employing, i.e., VUMAT for the modification of the fracture criteria [40], given that a
307 number of plasticity parameters need to be calibrated regardless the FEM approach adopted. In
308 view of defining a simplified and reliable modelling approach, a conventional failure was assumed
309 depending only by the maximum steel plastic strain of the chord in the joint region. This approach
310 allows the control of a single parameter for the calibration of the failure conditions based on
311 experimental results and can be considered reliable, as will be shown hereinafter.

312 To define the values that identify the failure, a parametric analysis was performed on CHS-8
313 and CFST-8 specimens. In detail, maximum plastic steel strain in the chord in the joint region was
314 varied until matching the experimental failure load. In other words, the experimental test for the
315 K-joints was reproduced by FE analysis without considering failure conditions in the FE model,
316 implementing the nominal steel constitutive mechanical law (yielding strain of 0.0015 for a yielding
317 stress of 311 MPa and rupture strain of 0.33 for a rupture stress of 425 MPa). In doing so, the
318 failure by punching shear, observed in correspondence of the connection between the steel chord
319 and the brace in tension, cannot be reproduced because it is attained for nominal strain lower than
320 rupture strain. By observing the values of the plastic strains in the joint region of the chord when the

load for the brace in tension in the specimens was equal (or near) the experimental one, this value was used as limit for the steel material, implementing in the constitutive law a stress drop (therefore as predictive analysis) and finding the failure load based on the assignment of the plastic strain limit above discussed. In this way, also the load recorded in the FE model did not increase because of the stress drop in the constitutive law.

To give an example, it is shown in Fig. 9(a) that the experimental failure load for CHS-8 specimen is reached for values of plastic strains around 0.025 instead of the value of rupture strain of the steel material. If this value is assigned to the constitutive law of the steel as a maximum steel strain, defining after this value a stress drop in the uniaxial stress-strain law, the analysis can be performed as predictive to find the maximum load for the brace in tension. At the same way, referring to the specimen CFST-8, Fig. 9(a) shows that the experimental failure load for CHS-8 specimen is reached for values of plastic strains around 0.085 instead of the value of rupture strain of the steel material. Also in this case, this value can be used to define a limit strain followed by a stress drop in the uniaxial stress strain law and performing the analysis to obtain the failure load.

In order to avoid the influence of the mesh size and obtain an optimal balance between accuracy in the reproduction of the results and time computational effort, several sensitivity analyses were performed to find the optimal dimensions of the meshes to be used in the model.

The load vs maximum steel strain in the chord and the load vs brace displacement are shown in Figs. 9(a) and (b), respectively. The results indicate that the stiffness of the experimental response was well reproduced by the FEM model both for the behavior in tension and in compression. Moreover, the failure for the joint in the tension zone was well reproduced both in terms of ultimate displacement and corresponding strength. It has to be stated that the recording of the displacement in the numerical model corresponded to the point of application of the displacement. On this frame, since the numerical simulation were performed displacement controlled, the response of the brace in compression was obtained for the same levels of displacements of the brace in tension, resulting

higher than the experimental results, carried out by force-controlled load path and therefore equal for both braces in compression and in tension.

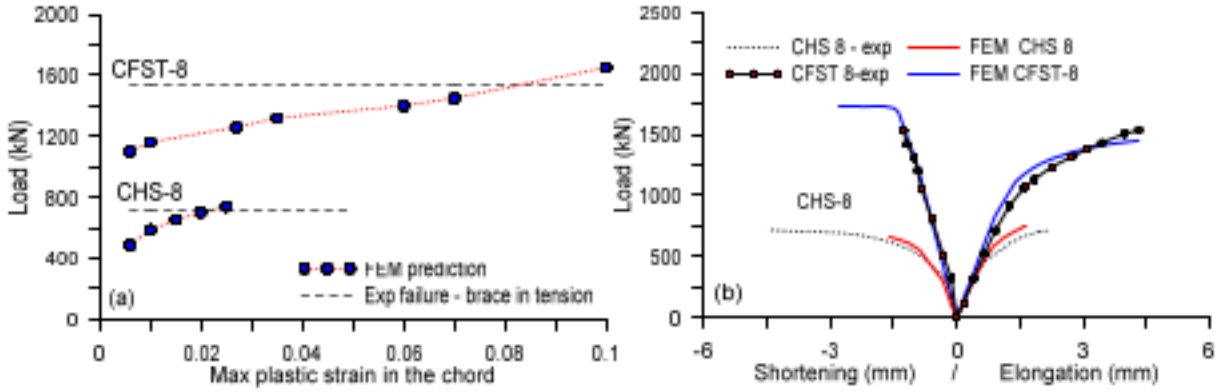

Fig. 9. (a) Calibration of failure conditions; (b) experimental - numerical comparisons for CHS-8 and CFST-8 K-joints specimens

4.2 FEM of CFST-8 and CFST-S specimens: actual and equivalent FE models

As previously discussed, the CFST K-joints can be further stiffened by the addition of studs welded to the interior surface of the chord in the joint region. Through the addition of studs, the chord section is better constrained by the infilled concrete and its deformation is therefore reduced. Therefore, the studs are able to further reduce peaks and non-uniformity of the strain distribution at the joint location in the chord and the brace members of CFST specimens with studs compared to those in CFST specimens without studs. This results in a better performance of the overall joint, exploiting the entire capacity of the members over the yielding stress conditions.

The FEM of such composite K-joints with studs is obviously expensive in terms of computational effort, by requiring high number of elements for the discretization of the studs and the holes in the concrete filling having the shape of the studs. In this frame, the following modelling procedure was proposed for the FEM of the actual and equivalent FE model composite K-joints:

- Actual FE model for CFST-S specimens: modelling of the K-joint with studs, steel hardening and friction coefficient along the contact surfaces. In doing so, a slice FE model was built to reduce the number of elements meshing and time computational effort.
- Equivalent FE model for CFST-S specimens: complete modelling of the K-joint, without including studs. The presence of the studs and the adding stiffness provided by them was supplied by employing cohesive interaction properties in the contact surfaces.

To show the importance and the usefulness of the above strategy, for example, in the frame of this study, the discretization of the CFST-8 specimen (dimensions of members reported in Table 1) required an optimal number of around 20600 quadratic tetrahedral elements of type C3D10 for the K-joint, including steel chord and steel braces, and 5100 linear hexahedral elements of type C3D8R, to a total number of around 25700 elements. In the case of the actual model, despite a slice modelling of around 1/3 of the total geometry, related to the joint region (see Figs. 6 and 7) the optimal number required to model the steel parts (chord, braces, and studs) and the concrete part were around 38900 and 83100 quadratic tetrahedral elements of type C3D10, respectively, to a total number of around 122000 elements. If, for example, a complete FE model should be built for CFST-8 S specimen, around 114245 and 739020 quadratic tetrahedral elements of type C3D10 are required to model the steel parts and the concrete part respectively, to a total number of around 853265 elements. It is immediately evident that, by adopting the proposed modelling approach, the modelling of the CFST-S K-joint with studs can be done by keeping the same number of elements used for the CFST K-joint, without the need to model studs, using only the 3% of elements compared to the actual model with a consequent high optimization of the time computational effort.

The results of the stress and the strain fields for the actual FE model of CFST-8 S specimen at failure conditions are shown in Figs. 10(a) and (b), respectively. It can be noted that, according to the experimental results by Huang et al. [9], the concentration of the strains (and consequently the increasing of the steel stress) was observed along the joint region of the weld toe of the brace in

389 tension. It has to be observed moreover that, for higher displacement levels, the brace in
390 compression exhibited bulge and local bucking. This can be also recognized in Fig. 3, where the
391 failure patterns observed from experimental tests are shown for the specimens with and without
392 studs as for Table 2, which summarizes the failure mechanism for each specimen.

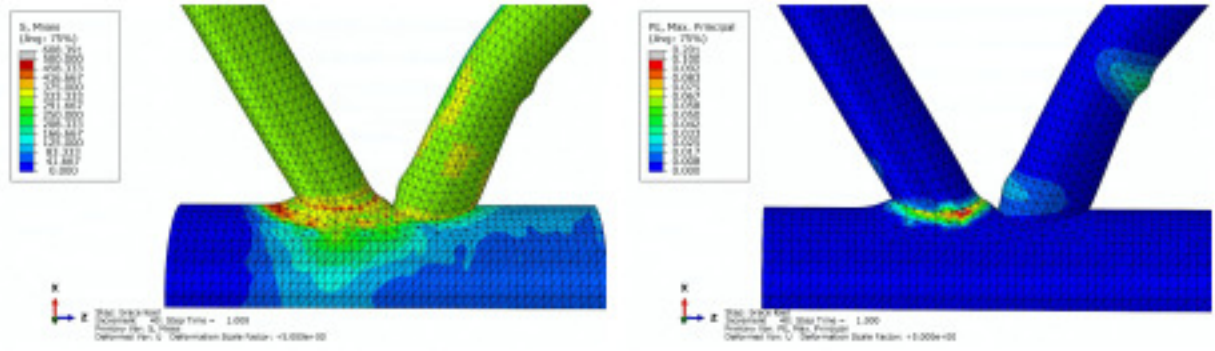

(a) (b)

Fig. 10. (a) Stress and (b) strain fields for CFST-8 S specimen

393 The positive role of the steel studs can be observed also in Figs. 11 (a) and (b) for the FE
394 models for CFST-8 and CFST-8 S specimens, respectively, in which the comparisons of the
395 distribution of the stress field indicate that the studs were able to increase the stiffness in the joint
396 region with the brace in tension, holding back the steel chord to the concrete filling by exploiting
397 the reaction of the steel studs.

398 By focusing the attention to the behavior in tension, the load vs displacement results of the FE
399 simulation are shown in Fig. 12 and compared with the corresponding experimental specimens. As
400 show in Fig. 12, the model resulted to be efficient and reliable in the prediction of the stiffness and
401 the load bearing capacity of the K-joint specimen CFST-8 S with studs. However, the
402 computational effort resulted very high due to the high number of finite elements used for the
403 meshing and consequently the computational time.

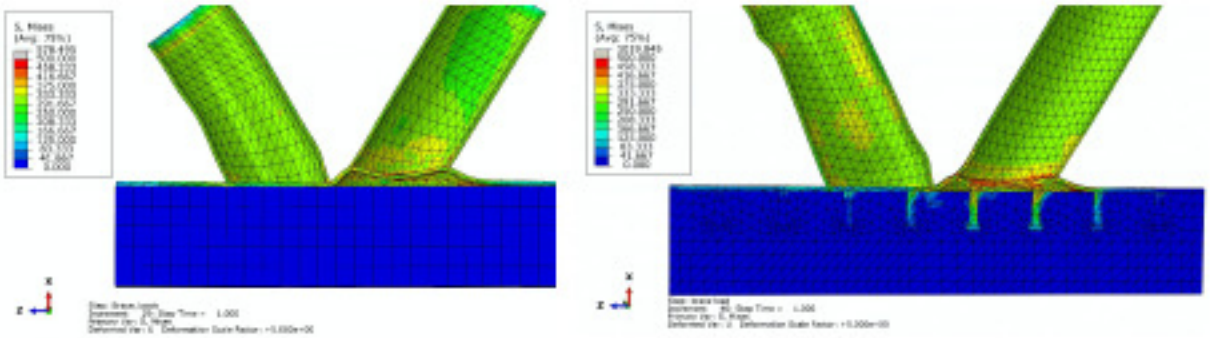

(a) (b)

Fig. 11. Stress fields for (a) CFST-8 specimen and (b) CFST-8 S specimen

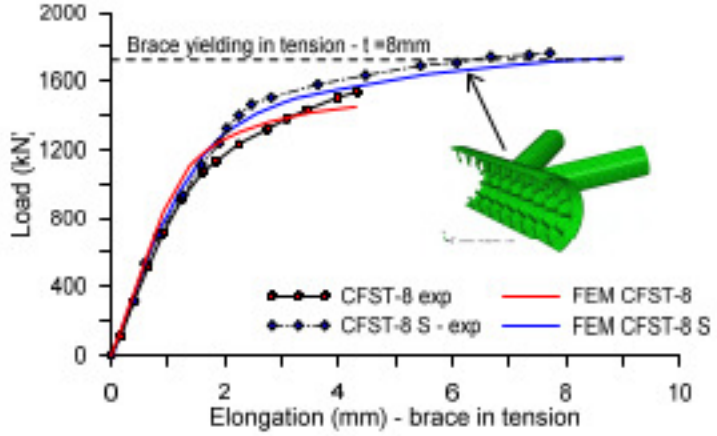

Fig. 12. Comparisons between actual FE model prediction and experimental results

In the frame of the simplified modelling of the CFST-S specimens, simulations were performed by employing cohesive interactions methods in the contact surfaces available in ABAQUS software package. Surface-to-surface contact (surface contact-based cohesive method) interaction was defined for the inner surface of the steel chord and the outer surface of the concrete, having cohesive behavior by "traction-separation behavior" defined only at the elastic stage (no failure) by specifying contact stiffness coefficients available in the cohesive properties for any slave node experiencing contact. Small sliding solving method was used, defining the stiffness parameters K_{nn}, K_{ss} and K_{tt}, respectively, for the normal and tangential stiffness between the inner surfaces of steel chord and the outer surface of concrete filling. The additional stiffness obtained by

415 the presence of the studs in the actual models was therefore supplied by assigning additional
416 stiffness to the interface by the cohesive stiffness coefficients.

417 A sensitivity analysis was performed to investigate on the influence of the stiffness coefficients
418 in the overall response of the CFST-S K-joints by varying the values from small to high stiffness.
419 The results are shown in Fig. 13. The aim was to find best fitting for the assumption of the optimal
420 values for the cohesive interaction stiffness coefficients in the equivalent model. In detail, the
421 analyses with cohesive coefficients were labeled with $c_{Knn\text{-}Kss\text{-}Ktt}$, and trial values of 2-2-2, 3-3-3,
422 5-5-5 and 10-10-10 were assigned. In addition, to define upper and lower bound, analyses were
423 performed also in the cases of perfect contact between the surfaces, defined by "tie-interaction
424 properties" and in the case of no friction nor cohesive properties, by defining "friction interaction"
425 between the contact surfaces. The best fitting was found for case analysis $c_{3\text{-}3\text{-}3}$ and adopted in the
426 subsequent analyses for the other K-joint specimens.

427 The trial analyses highlighted that the value assumed for the contact stiffness coefficients can
428 be related to the density of the studs, that is the number and the geometrical arrangement of them in
429 the inner surface of the steel chord. It has to be stated that the adopted values are therefore suitable
430 for the arrangement used to build up the specimens analyzed in this study, and, for other densities of
431 the studs, the optimal values for the contact stiffness coefficients need to be re-calibrated. This
432 aspect can be focused by performing parametric analysis by varying geometrical and mechanical
433 properties of the CFST K-joint specimens as well as different densities of the studs and finding
434 empirical relationships that link the values to be used for the contact stiffness coefficient to the
435 density of the studs, and it can be object of investigation for future studies.

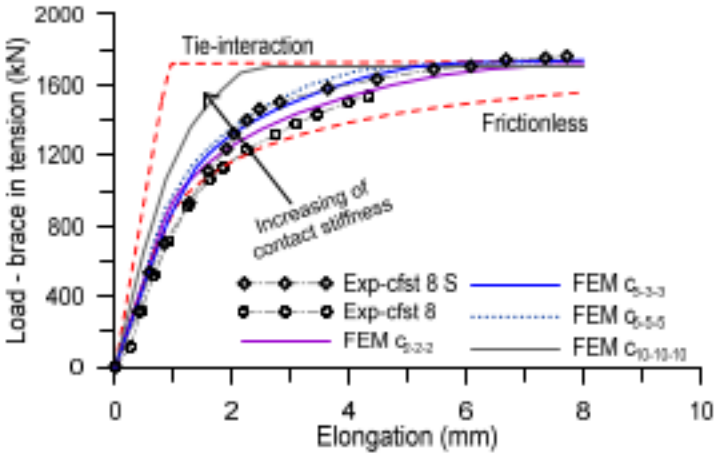

436

437 Fig. 13. Comparisons between equivalent FE model prediction and experimental results

438

439 **4.3 Comparisons between equivalent FE model prediction and experimental results**

440 The results of the above-described procedure for the definition of the FEM strategy and the
441 assumption of the optimal parameters to reproduce the stiffness and the strength capacity of CFST
442 and CFST S specimens were used for the comparisons with other experimental results. In detail, the
443 parameters used for the calibration of CFST-8 and CFST-8 S specimens were adopted as predictive
444 approach in the FE models for the other specimens by Huang et al. [9] and Liu et al. [18].

445 Comparisons between FE prediction and experimental results in terms of strength are shown in
446 Fig. 14, where it is possible to denote that the difference is the results were always below the 10%.
447 Some difference slightly over the 10% was related to the prediction of the behavior for the brace in
448 compression, for the reasons related to the numerical simulations displacement-controlled discussed
449 in the previous sections.

450 The load vs displacement response between FE prediction and experimental results are shown
451 in Figs. 15(a)-(d) for the specimens by Huang et al. [9] and Liu et al. [18], respectively. Overall, the
452 FE model resulted reliable in the reproduction of the strength for all the specimens. Small
453 differences in the stiffness were observed in some cases, where the FE model resulted to have

slightly higher stiffness. These differences can be related to experimental uncertainties (this can be stated because of the description of the consistency of the FE results above discussed).

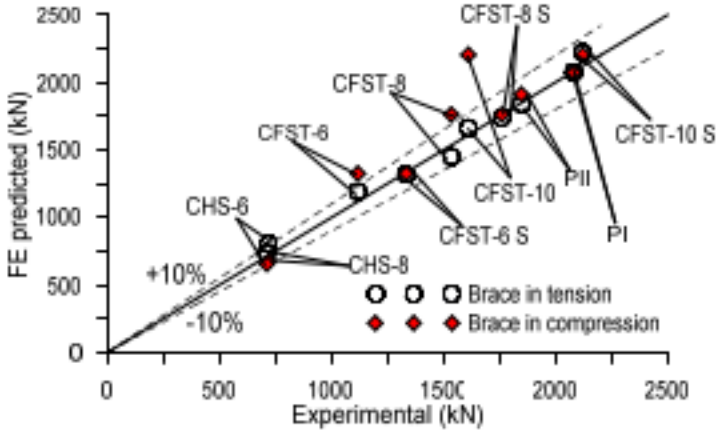

Fig. 14. Comparisons between equivalent FE model prediction and experimental results in terms of strength.

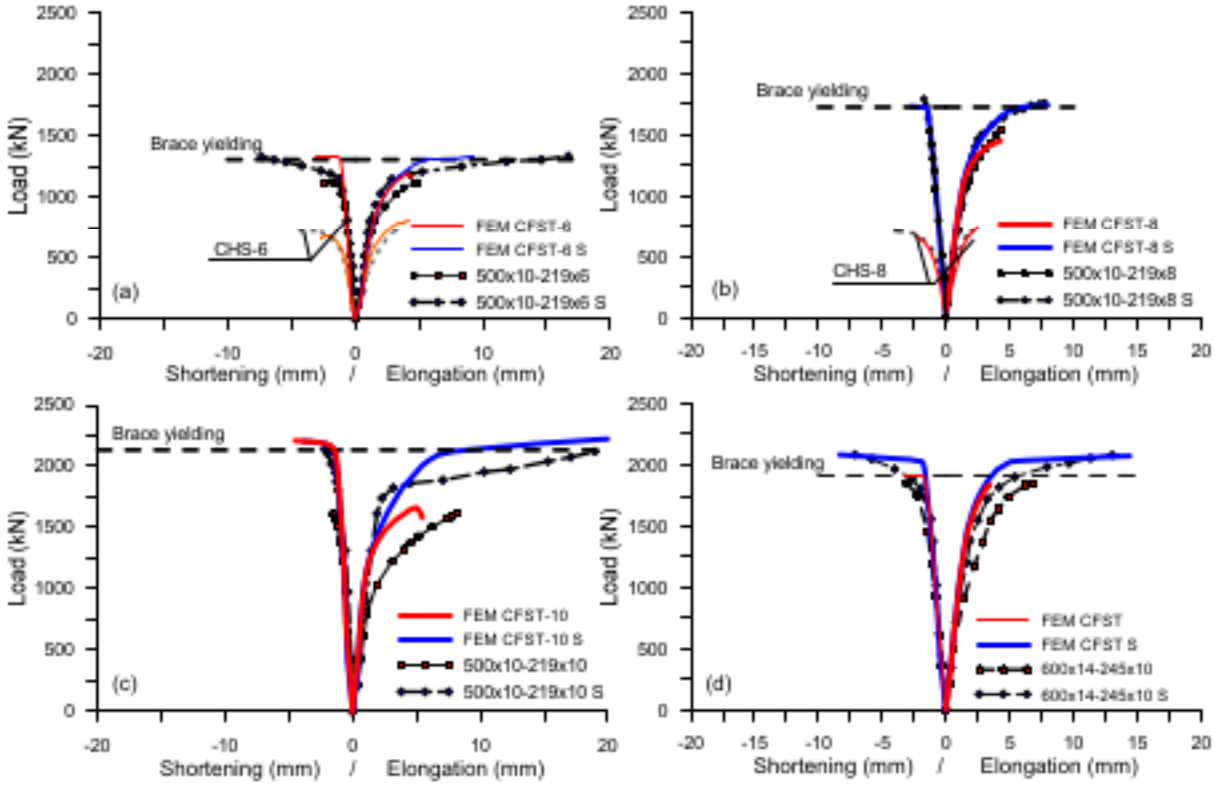

Fig. 15. Comparisons between equivalent FE model prediction and experimental results: (a), (b) and (c) specimens by Huang et al. [9]; (d) specimens by Liu et al. [18].

462 The consistency of the FE results in the reproduction of the overall behavior of the K-joint was
463 confirmed by the comparisons of the numerical curves related to the braces in tension, shown in Fig.
464 16. Given that the geometry of the steel chord was kept the same for all the specimens, an important
465 parameter to be assumed as indicator of the performances of the K-joints can be the thickness to
466 diameter ratio (t_b) of the braces, which determines the strength and stiffness of the
467 load-displacement response. It can be noted that the CFST-6 specimen (t/d = 0.274) exhibited
468 ultimate load near to the yielding point of the steel brace in tension. The presence of the studs
469 influenced slightly the strength: in detail, 1192 kN and 1325 kN were ultimate loads for the CFST-6
470 and CFST-6 S, respectively, corresponding to increasing of around 11%. On the other hand, the
471 studs improved considerably the ductility of the K-joint. For the CFST-8 and CFST-8 S specimens
472 (t/d = 0.365), the strength improvement was more efficient, because the ultimate loads were 1448
473 kN and 1739 kN, respectively, with a strength increasing of around 20%. Finally, for the specimens
474 CFST-10 and CFST-10 S (t/d = 0.456) resulted again higher than the other cases. In detail, the
475 ultimate loads were 1662 kN and 2222 kN, respectively, with a strength increasing of around 33%.
476 These differences, as discussed in the previous section, were related to the fact that all the
477 specimens with studs reached at least the yielding conditions for the brace in tension. The yielding
478 load was not reached for the specimens without studs, were the failure (identified by punching shear)
479 is reached after the yielding of the brace. All the above considerations can be used as basis to
480 further highlight the positive role of the concrete filling coupled with the steel studs.

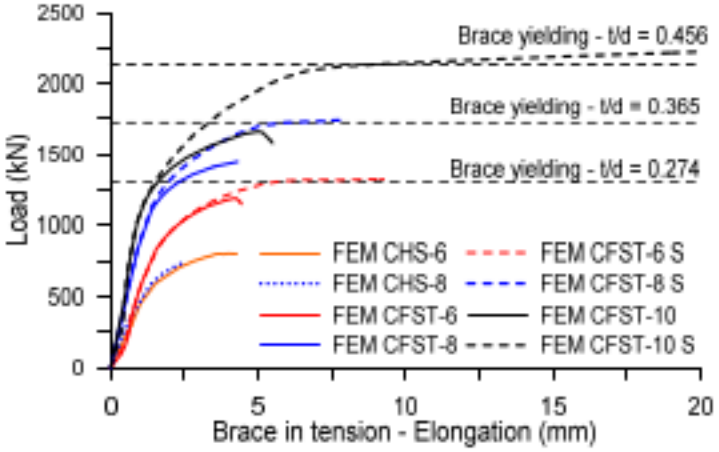

Fig. 16. Simplified equivalent FE model results of specimens by Huang et al. [9].

Conclusions

In this paper, a strategy for the FEM was presented for the reproduction of the stiffness and the strength capacity of CFST K-joints with and without steel studs welded in the inner surface of the chord in the joint region. The aim of the study was also to provide a simplified FEM approach to overcome the high time-computational costs required by the actual complex FE models keeping the same accuracy. Based on the results gained in the frame of the paper, the following conclusion can be summarized:

(1) The modelling issues related to the optimal assumptions and parameters to be used for a reliable modelling of such composite joints were discussed throughout the paper for each case of analysis. The FE modeling recommendation for CFST K-joints are then listed below:

- Modelling of steel chord and steel braces including i) hardening effects, ii) geometrical non-linearities for the members;
- Modelling of the concrete including non-linear behavior if the level of concrete stresses are higher than 50% of the concrete strength;
- Modelling of the contact surfaces between steel and concrete by assuming hard contact in the normal direction and Coulomb-friction law with a friction coefficient of 0.5 in the tangential

direction.

(2) For the CFST K-joints with studs, it was found that it is possible to employ cohesive-interaction properties by using the contact stiffness coefficients for the normal and the tangential directions to reproduce the contribution provided by the studs in the overall response of the joint. The values of the stiffness coefficients can be related to the density of the studs used to strengthen the inner surface of the chord in the joint region. In doing so, time-computational costs resulted to be extremely reduced.

(3) The modelling strategy presented, calibrated and validated against experimental results available in the state of the art, can be used for successive studies as predictive approach to calculate, by FE models, the stiffness and the strength capacity of such composite K-joints, covering a wide range of geometrical and mechanical properties.

CRediT authorship contribution statement

Marco Filippo Ferrotto: Data curation; Investigation; Methodology; Software; Visualization; Writing - original draft. **Luigi Fenu**: Conceptualization; Investigation; Methodology; Resources; Supervision; Writing - review & editing. **Junqing Xue**: Funding acquisition; Investigation; Methodology; Software; Visualization; Writing - original draft; Writing - review & editing. **Bruno Briseghella**: Conceptualization; Funding acquisition; Methodology; Project administration; Resources; Supervision; Writing - review & editing. **Baochun Chen**: Conceptualization; Funding acquisition; Supervision; Writing - review & editing. **Liborio Cavaleri**: Conceptualization; Methodology; Resources; Software; Supervision; Writing - review & editing.

Declaration of Competing Interest

The authors declare that they have no known competing financial interests or personal relationships that could have appeared to influence the work reported in this paper.

Acknowledgment

This work is supported by the National Natural Science Foundation of China [Grant Nos. 51778148, 51508103 and 52078136] and the Recruitment Program of Global Experts Foundation (TM2012-27).

References

[1] Chen BC, Wang TL. Overview of concrete filled steel tube arch bridges in China, Pract. Period. Struct. 2009; 14(2): 70–80, https://doi.org/10.1061/(ASCE)1084-0680(2009)14:2(70).

[2] Uy B. Applications, behaviour and design of composite steel-concrete structures, Adv. Struct. Eng. 2012; 15(9): 1559–1572, https://doi.org/10.1260/1369-4332.15.9.1559.

[3] Han LH, Li W, Bjorhovde R, Developments and advanced applications of concrete-filled steel tubular (CFST) structures: Members, J. Constr. Steel Res. 2014; 100: 211–228, https://doi.org/10.1016/j.jcsr.2014.04.016.

[4] Tian ZJ, Liu YJ, Jiang L, Zhu WQ, Ma YP. A review on application of composite truss bridges composed of hollow structural section members, J. Traffic. Transp. Eng. 2019; 6(1): 94–108, https://doi.org/10.1016/j.jtte.2018.12.001.

[5] Wang ZB, Zhong T, Han LH, Uy B, Lam D, Kang WH. Strength, stiffness and ductility of concrete-filled steel columns under axial compression, Eng. Struct. 2017; 135: 209–221, https://doi.org/10.1016/j.engstruct.2020.111599.

[6] Wu QX, Yoshimura M, Takahashi K, Nakamura S, Nakamura T. Nonlinear seismic properties of the Second Saikai Bridge: A concrete filled tubular (CFT) arch bridge, Eng. Struct. 2006; 28(2): 163–182, https://doi.org/10.1016/j.engstruct.2005.05.003.

[7] Xue JQ, Briseghella B, Chen BC, Effects of debonding on circular CFST stub columns, J. Constr. Steel Res. 2012; 69: 64–76, https://doi.org/10.1016/j.jcsr.2011.08.002.

547 [8] Yadav R, Yuan HH, Chen BC, Lian ZB, Experimental study on seismic performance of latticed
548 CFST-RC column connected with RC web, Thin-Walled Struct. 2018; 126: 258–265,
549 https://doi.org/10.1016/j.tws.2017.11.043.
550 [9] Huang WJ, Fenu L, Chen BC, Briseghella B. Experimental study on K-joints of concrete-filled
551 steel tubular truss structures, J. Constr. Steel Res. 2015; 107: 182–193,
552 https://doi.org/10.1016/j.jcsr.2015.01.023.
553 [10] Huang YH, Liu AR, Fu JY, Pi Y.L. Experimental investigation of the flexural behavior of
554 CFST trusses with interfacial imperfection, J. Constr. Steel Res. 2017; 137: 52–65,
555 https://doi.org/10.1016/j.jcsr.2017.06.009.
556 [11] Huang WJ, Fenu L, Chen BC, Briseghella B. Experimental study on joint resistance and failure
557 modes of concrete filled steel tubular (CFST) truss girders, J. Constr. Steel Res. 2018; 141:
558 241–250, https://doi.org/10.1016/j.jcsr.2017.10.020.
559 [12] Ma YP, Liu YJ, Ma TY, Zafimandimby M. Flexural Stiffness of Rectangular Hollow Section
560 (RHS) Trusses, Eng. Struct. 2021; 239: 112336, https://doi.org/10.1016/j.engstruct.2021.112336.
561 [13] Chen SL, Hou C, Zhang H, Han LH, Mu TM. Reliability-based evaluation for concrete-filled
562 steel tubular (CFST) truss under flexural loading, J. Constr. Steel Res. 2020; 169: 106018,
563 https://doi.org/10.1016/j.jcsr.2020.106018.
564 [14] Wei JG, Luo X, Lai ZC, Varma AH. Experimental behavior and design of high-strength
565 circular concrete-filled steel tube short columns. J. Struct. Eng. 146 (1) (2020) 04019184,
566 https://doi.org/10.1061/(ASCE)ST.1943-541X.0002474.
567 [15] Xue JQ, Fiore A, Liu ZH, Briseghella B, Marano GC, Prediction of ultimate load capacities of
568 CFST columns with debonding by EPR, Thin-Walled Struct. 2021; 164: 107912,
569 https://doi.org/10.1016/j.tws.2021.107912.

570 [16] Wei JG, Xie ZT, Zhang W, Luo X, Yang Y, Chen BC. Experimental study on circular steel
571 tube-confined reinforced UHPC columns under axial loading, Eng. Struct. 2021; 230: 111599,
572 https://doi.org/10.1016/j.engstruct.2020.111599.
573 [17] Sakai Y, Hosaka T, Isoe A, Ichikawa A, Mitsuki K. Experiments on concrete filled and
574 reinforced tubular K-joints of truss girder, J. Constr. Steel Res. 2004; 60: 683–699,
575 https://doi.org/10.1016/S0143-974X(03)00136-6.
576 [18] Liu JP, Chen JK, Chen BC. Experimental studies on load-transferring mechanism of CFST
577 directly-welded K-joint with studs, Eng. Mech. 2017; 34(9): 150–157,
578 https://doi.org/10.6052/j.issn.1000-4750.2016.05.0336, [in Chinese].
579 [19] Hou C, Han LH, Mu TM. Behaviour of CFDST chord to CHS brace composite K-joints:
580 Experiments, J. Constr. Steel Res. 2017; 135: 97–109. https://doi.org/10.1016/j.jcsr.2017.04.015.
581 [20] Hou C, Han LH. Analytical behaviour of CFDST chord to CHS brace composite K-joints, J.
582 Constr. Steel Res. 2017; 128: 618–632, https://doi.org/10.1016/j.jcsr.2016.09.027.
583 [21] Jin DYD, Hou C, Shen LM, Han LH. Numerical performance of blind-bolted demountable
584 square CFST K-joints, J. Build. Eng. 2021; 33: 101646,
585 https://doi.org/10.1016/j.jobe.2020.101646.
586 [22] Zheng J, Nakamura S, Okumatsu T, Nishikawa T. Formulation of stress concentration factors
587 for concrete filled steel tubular (CFST) K-joints under three loading conditions without shear
588 forces, Eng. Struct. 2019; 190: 90–100, https://doi.org/10.1016/j.engstruct.2019.04.017.
589 [23] Hou C, Han LH, Zhao XL. Concrete-filled circular steel tubes subjected to local bearing force:
590 Experiments, J. Constr. Steel Res. 2013; 83: 90–104. https://doi.org/10.1016/j.jcsr.2013.01.008.
591 [24] Hou C, Han LH, Zhao XL. Concrete-filled circular steel tubes subjected to local bearing force:
592 Finite element analysis, Thin-Walled Struct. 2014; 77: 109–119,
593 https://doi.org/10.1016/j.tws.2013.12.006.

[25] Zeng J, Nakamura S, Ge Y, Chen KM, Wu QX. Formulation of stress concentration factors for concrete-filled steel tubular (CFST) T-joints under axial force in the brace, Eng. Struct. 2018; 170: 103–117. https://doi.org/10.1016/j.engstruct.2018.05.066.

[26] Huang YF, Briseghella B, Zordan T, Wu QX, Chen BC. Shaking table tests for the evaluation of the seismic performance of an innovative lightweight bridge with CFST composite truss girder and lattice pier, Eng. Struct. 2014; 75: 73–86, https://doi.org/10.1016/j.engstruct.2014.05.039.

[27] Xu W, Han LH, Tao Z. Flexural behaviour of curved concrete filled steel tubular trusses, J. Constr. Steel Res. 2014; 93: 119–134, https://doi.org/10.1016/j.jcsr.2013.10.015.

[28] Yuan HH, Wu QX, Huang YF, She ZM. Experimental and theoretical studies on the seismic performance of CFST battened built-up column piers, Eng. Struct. 2020; 206: 110099, https://doi.org/10.1016/j.engstruct.2019.110099.

[29] European Committee for Standardization, EN 1993-1-8: Eurocode 3: Design of steel structure - Part 1-8: Design of joints, Brussels, Belgium, 2007.

[30] ABAQUS 6.14-1 Documentation, Dassault Systèmes, Simulia, Providence, RI, 2014.

[31] Ferrotto MF, Cavaleri L, Trapani FD. FE modeling of Partially Steel-Jacketed (PSJ) RC columns using CDP model, Comput. Concrete. 2018; 22(2): 143–152, https://doi.org/10.12989/cac.2018.22.2.143.

[32] Han LH, Yao GH, Tao Z. Performance of concrete-filled thin-walled steel tubes under pure torsion, Thin-Walled Struct. 2007; 45(1): 24–36, https://doi.org/10.1016/j.tws.2007.01.008.

[33] Lai M, Hanzic L, Ho JCM. Fillers to improve passing ability of concrete. Structural Concr. 2018; 1-13. https://doi.org/10.1002/suco.201800047.

[34] Lai M, Hanzic L, Ho JCM. A theoretical axial stress-strain model for circular concrete-filled-steel-tube columns. Eng. Struct. 2016; 125, 124–143.

[35] Kwan AKH, Dong CX, Ho JCM. Axial and lateral stress–strain model for FRP confined concrete. Eng. Struct. 2015; 99, 285–295.

[36] Lai MH, Ho JCM. Effect of continuous spirals on uni-axial strength and ductility of CFST columns. J. Constr. Steel Res. 2015; 104, 235–249.

[37] Lai MH, Ho JCM. Confinement effect of ring-confined concrete-filled-steel-tube columns under uni-axial load. Eng. Struct. 2014; 67, 123–141.

[38] Dong CX, Kwan AKH, Ho JCM. A constitutive model for predicting the lateral strain of confined concrete. Eng. Struct. 2015; 91, 155–166.

[39] Tao Z, Wang ZB, Yu Q. Finite element modelling of concrete-filled steel stub columns under axial compression. J. Constr. Steel Res. 2013; 89, 121-131.

[40] Xu F, Chen J, Jin WL. Punching shear failure of concrete-filled steel tubular CHS connections, J. Constr. Steel Res. 2016; 124: 113–121, https://doi.org/10.1016/j.jcsr.2016.05.010.